5 Multi-Scale Modeling in Solid–Liquid Phase Change Conjugate Heat Transfer for Thermal Energy Storage Applications

Qinlong Ren, Li Chen, Yu-Bing Tao, and Wen-Quan Tao
Xi'an Jiaotong University

CONTENTS

5.1 Introduction 98
5.2 Multi-Scale Numerical Methods and Coupling Schemes 101
5.2.1 Molecular Dynamics Simulation 101
5.2.1.1 Common Used Force Field 101
5.2.2 Lattice Boltzmann Method 103
5.2.2.1 Governing Equations for Solid–Liquid Phase Change Conjugate Heat Transfer 103
5.2.2.2 MRT Enthalpy-Based LBM in 2D Cartesian Coordinate 104
5.2.2.3 MRT Enthalpy-Based LBM in 3D Cartesian Coordinate 107
5.2.2.4 Numerical Reconstruction of Porous Media 109
5.2.2.5 Graphic Processor Units (GPUs) Computing 110
5.2.3 Finite Volume Method 111
5.2.4 LBM-FVM Coupling Schemes 112
5.3 Applications of Multi-Scale Modeling to Latent Heat Thermal Energy Storage 114
5.3.1 Thermophysical Properties of PCMs 115
5.3.1.1 Specific Heat Capacity and Melting Enthalpy 115
5.3.2 Pore-Scale Modeling of LHS System 115
5.3.3 Representative Elementary Volume Scale Modeling of LHS System 117
5.4 Conclusions 119
Acknowledgments 120
References 120

DOI: 10.1201/9781003213260-5

5.1 INTRODUCTION

Solar energy becomes a promising alternative for overcoming the shortage of fossil energy and world environmental pollution during the past decades. However, the intermittent nature of solar energy limits its flexible large-scale applications. Thermal energy storage (TES) offers an indispensable bridge between the solar energy conversion and utilization at different peak periods [1]. Generally, the TES technologies are classified into sensible heat storage systems, latent heat storage (LHS) systems, and chemical heat storage systems. Based on the advantages of high energy storage density and nearly constant operating temperature, LHS system is attractive for storing solar thermal energy through solid–liquid phase change [2,3]. Under this situation, the heat transfer capability of LHS system plays an essential role in its energy storage efficiency. Nevertheless, the thermal conductivity of phase change materials (PCMs) is usually low, impeding the corresponding heat absorption and release rates in the LHS system. Facing this scientific challenge, effectively enhancing the solid–liquid phase change conjugate heat transfer is an inevitable task for the practical applications of LHS units in the renewable solar thermal energy system.

To ameliorate the thermal behavior of LHS system, several heat transfer enhancement technologies are developed in recent years including adding nanoparticles, using extended fins, and inserting porous media [4,5]. When nanoparticles such as carbon nanotubes, graphite, graphene, metal, and metal oxide are dispersed into the PCMs, the thermophysical properties of nano-enhanced PCMs including thermal conductivity, latent heat capacity, melting temperature, density, and viscosity are obviously altered [6]. Specifically, due to the nanoparticle clustering phenomenon, the nano-enhanced PCMs usually exhibit higher thermal conductivity than that predicted by the effective medium theories [7], making them convincing for improving thermal performance of LHS system. However, the existence of nanoparticles also increases the viscosity of PCMs [8], significantly weakening the convective heat transfer. Besides, the thermal stability of nano-enhanced PCMs is also challenging because the dispersed nanoparticles confront aggregation and sedimentation during charging and discharging cycles of LHS system, limiting the lifetime and robustness of nano-enhanced PCMs [9]. Alternatively, due to the simple fabrication and low construction cost, high thermal conductive extended fins with numerous geometries like longitudinal, circular/annular, plate, pin, and biomimetic tree shape are widely inserted into the LHS system to consolidate its heat transfer capability [10]. Even though the extended fins enhance the heat transfer area with improved energy storage rate, it also attenuates the energy storage capacity of LHS system to some extent. Furthermore, despite that the prolonged fin length in LHS system strengthens the heat transfer depth, the fin efficiency is commonly decreased due to its reduced inside temperature [11]. Under this circumstance, the extended fin configurations need to be optimized in consideration of the conjugate heat transfer occurring on the interface between fins and PCMs to maximize the thermal response of LHS system. On the other hand, diversified porous media with high thermal conductivity such as metal foams, metal fiber felts, expanded graphite, and graphite foam are integrated into the LHS system to accelerate its thermal response behavior [12]. Due to the interconnected high-speed conductive heat transfer channels inside porous media,

the effective thermal conductivity of porous medium-PCM composites is obviously improved [13]. Nevertheless, when the porous media exist in the LHS system, the convective heat transfer of PCMs is depressed due to the porous medium skeleton induced limited space for fluid flow development. Similar to the use of extended fins, the energy storage capacity of porous medium-PCM composites is reduced with their decreased porosity [14]. Besides, the gas void cavities are generated by the notable volume variation of PCMs during melting and solidification, affecting the conjugate heat transfer process inside the LHS system [15]. Furthermore, the contact thermal resistance between porous media and PCMs also influences their conjugate heat transfer rate. Hence, the morphology and thermophysical property of porous media require careful design when they are applied to enhance the thermal response ability of LHS system. The aforementioned discussions show that the heat transfer enhancement techniques for LHS system always exhibit the outstanding advantages simultaneously accompanied by several drawbacks. Therefore, heat transfer optimization becomes necessary for the LHS system to balance its energy storage efficiency and energy storage capacity in order to modulate various trade-off effects.

Due to the advantages of high flexibility and low cost compared with experimental measurements, multi-scale modeling is a powerful tool to investigate diverse heat and mass transfer processes in engineering fields [16–18]. In multi-scale modeling, the physical nature at different scales is fully considered and utilized such as molecular dynamics (MD) simulation at atomic scale, lattice Boltzmann method (LBM) at mesoscopic scale, and finite volume method (FVM) at macroscopic scale to solve the various governing equations in different regions. Then, the complicated transport phenomena are coupled through particular mathematical schemes at the interfacial boundaries between MD-LBM [19], MD-FVM [20], and LBM-FVM [21,22]. Due to its atomic characteristic, MD simulation is convincing for exploring the microscopic phenomena and thermophysical properties of PCMs including melting/freezing point, thermal conductivity, latent heat, and viscosity [23]. The melting/freezing point of PCMs is essentially computed through interface method [24] and void method [25] because of its significant influence on solid–liquid phase change during TES. Moreover, the thermal conductivity of PCMs could be calculated by equilibrium molecular dynamics (EMD) simulation [26,27] and non-equilibrium molecular dynamics (NEMD) simulation [28,29]. Therefore, the thermophysical properties of PCMs achieved by distinct MD simulations offer important foundations for investigating the latent heat TES process with different heat transfer enhancement technologies at mesoscopic and macroscopic scales.

Based on its mesoscopic kinetic nature and parallel characteristic, LBM is becoming a powerful numerical method to simulate complicated heat transfer and fluid flow phenomena [30,31]. The existing lattice Boltzmann models for solid–liquid phase change heat transfer could be generally classified into three categories: (1) the phase-field method [32,33], (2) the enthalpy-based method [34], and (3) the immersed boundary method [35]. For the phase-field-based LBM, the solid–liquid interface is implicitly tracked by an auxiliary parameter which smoothly varies across the diffusive phase interface. Consequently, extremely fine grids are required in the interfacial region. In addition, when the immersed boundary-based LBM is applied to simulate the solid–liquid phase change heat transfer, the solid–liquid interface is explicitly

tracked by the Lagrangian nodes, while the temperature and fluid flow fields are solved on the Eulerian nodes. However, the interpolation process of physical variables between Lagrangian nodes and Eulerian nodes dramatically burdens the computational load. Alternatively, the enthalpy-based LBM becomes the most robust and efficient approach for investigating solid–liquid phase change conjugate heat transfer. Originally, the enthalpy-based LBM is developed by Jiaung et al. for heat conduction with solid–liquid phase change [36]. Even though their simulation of solid–liquid phase change heat conduction at a constant melting temperature with mushy zone is demonstrated to be consistent with analytical or previous numerical results, iteration steps for the non-linear latent heat source are necessary. To avoid the iteration of latent heat source term, Eshraghi and Felicelli derived an implicit enthalpy-based LBM scheme for heat conduction with solid–liquid phase change through solving a linear system of equations [37]. However, numerically solving a linear system of equations at each time step also decreases the computational efficiency. Through modifying the equilibrium distribution function for temperature, Huang et al. successfully developed a two-dimensional (2D) single-relaxation-time (SRT) enthalpy-based LBM for solid–liquid phase change heat transfer without iteration of latent heat source or solving a linear system of equations [38]. Under this situation, the computational efficiency of LBM for simulating solid–liquid phase change is obviously improved. However, the SRT enthalpy-based LBM suffers from the drawback of numerical instability, and the specific heat and thermal conductivity could not be individually decoupled from the relaxation time, limiting its application for handling coupled Dirichlet–Neumann conditions in the conjugate heat transfer. To overcome these shortcomings, Huang et al. further developed a 2D multiple-relaxation time (MRT) enthalpy-based LBM to reduce the numerical diffusion during solid–liquid phase change, and the specific heat and thermal conductivity are also decoupled with each other to guarantee the continuity of heat transfer at the interface between different materials [39]. Afterwards, several different MRT enthalpy-based LBM schemes are developed for solid–liquid phase change heat transfer including axisymmetric cylindrical model [40], axisymmetric spherical model [41], and three-dimensional (3D) Cartesian model [42] as well as its representative elementary volume (REV) scale model in porous media [43]. Particularly, the enthalpy-based LBM considering contact thermal resistance is also developed making it more appropriate to investigate the solid–liquid phase change conjugate heat transfer in the practical LHS system [44]. Based on the tremendous efforts, the enthalpy-based LBM is widely used to optimize the thermal performance of LHS system especially for pore-scale clarifying the conjugate heat transfer inside complicated porous medium-PCM composites through reconstructing their diverse morphologies by X-ray computed tomography [45] or numerical methods [46–49]. Furthermore, the graphic processor units (GPUs) computing becomes attractive in recent years, and the enthalpy-based LBM is also successfully fitted onto GPUs to achieve parallel simulation with high computational acceleration ratio [50–51], making LBM more powerful for designing the thermal performance of LHS system.

Besides, with the continuous development during the past half century, FVM is robust for computational fluid dynamics (CFD) and heat transfer problems [52]. In particular, FVM is also applied to model solid–liquid phase change heat transfer

in solar TES systems [53]. Based on the IDEAL algorithm [54], Li et al. derived an FVM with consideration of non-Darcy effect, local natural convection, and thermal non-equilibrium for solid–liquid phase change conjugate heat transfer in porous medium-PCM composite [55]. In addition, Ling et al. developed a sharp-interface-based FVM with SIMPLER algorithm to simulate solid–liquid phase change heat transfer [56]. The solid–liquid interface is captured by combing volume-of-fluid (VOF) and level-set (LS) methods (VOSET), and the interaction between solid and liquid phases is handled by an immersed boundary method (IBM). Furthermore, as a commonly used FVM-based CFD commercial software, ANSYS Fluent is also widely used for designing the thermal behavior of LHS system with different heat transfer enhancement technologies for practical engineering applications [57–59]. From the aforementioned discussions, multi-scale modeling is an effective technique for optimizing the thermal response of LHS system. In this chapter, we highlight the multi-scale numerical methods for solid–liquid phase change conjugate heat transfer.

5.2 MULTI-SCALE NUMERICAL METHODS AND COUPLING SCHEMES

Multi-scale modeling takes the advantages of various numerical methods at different scales to investigate the complicated physical phenomena with high efficiency. In this section, the MD simulation for computing thermophysical properties of PCMs is firstly discussed. Then, the enthalpy-based MRT LBM in 2D and 3D Cartesian coordinates is elaborated, respectively. Besides, the reconstructing methodologies for porous media and the principle of GPUs computing are further presented. Then, the FVM is briefly introduced, and the coupling scheme between LBM and FVM is finally analyzed.

5.2.1 Molecular Dynamics Simulation

MD simulation is a powerful tool for the prediction of thermophysical properties of PCMs and the solid–liquid interface interactions during melting and solidification processes [60–62]. The microphysical model of PCMs is often constructed by common modeling tools, such as Materials Studio [63] or visual molecular dynamics (VMD) software [64]. Then, the MD simulations can be performed with software including Material studio or large-scale atomic/molecular massively parallel simulator (LAMMPS) package.

5.2.1.1 Common Used Force Field

The molecular force field is a functional model describing the potential energy interaction between the atoms in PCM, which is also known as potential energy function. In the classical MD, the potential energy function plays a vital role because it is closely related to the micro-motion of atoms, which directly affects the accuracy of simulation results. For the MD simulation of PCMs, it is important to select the suitable force field. In this section, the commonly used force fields for PCM are introduced.

a. CHARMM Potential

CHARMM is used to describe the interaction of organic systems, such as paraffin-based PCM. The pair styles compute Lennard Jones (LJ) and Coulomb interactions with additional switching or shifting functions that ramp the energy and/or force smoothly to zero between an inner and outer cutoff, which can be written as follows [61,62]:

$$E_{vdw}=\begin{cases}\mathrm{LJ}(r) & r<r_{\mathrm{in}}\\ S(r)\times\mathrm{LJ}(r) & r_{\mathrm{in}}<r<r_{\mathrm{out}}\\ 0 & r>r_{\mathrm{out}}\end{cases} \tag{5.1}$$

$$E_{\mathrm{coul}}=\begin{cases}C(r) & r<r_{\mathrm{in}}\\ S(r)\times C(r) & r_{\mathrm{in}}<r<r_{\mathrm{out}}\\ 0 & r>r_{\mathrm{out}}\end{cases} \tag{5.2}$$

$$\mathrm{LJ}(r)=4\varepsilon\left[\left(\frac{\sigma}{r}\right)^{12}-\left(\frac{\sigma}{r}\right)^{6}\right] \tag{5.3}$$

$$C(r)=\frac{Cq_iq_j}{\varepsilon r} \tag{5.4}$$

$$S(r)=\frac{\left[r_{\mathrm{out}}^2-r^2\right]^2\left[r_{\mathrm{out}}^2+2r^2-3r_{\mathrm{in}}^2\right]}{\left[r_{\mathrm{out}}^2-r_{\mathrm{in}}^2\right]^3} \tag{5.5}$$

where E_{vdw} is the van der Waals energy and E_{coul} is the electrostatic energy. $S(r)$ is the energy switching function. In addition, r_{in} and r_{out} represent the start distance and the end distance of the switching function, respectively.

$$E_{\mathrm{bond}}=K_b(b-b_0)^2 \tag{5.6}$$

$$E_{\mathrm{angle}}=K_\theta(\theta-\theta_0)^2+K_{\mathrm{ub}}(r-r_{\mathrm{ub}})^2 \tag{5.7}$$

The angle style uses an additional Urey-Bradley angle term based on the distance between the first and third atoms in the angle.

$$E_{\mathrm{dihedral}}=K_\chi(1+\cos(n\chi-\delta)) \tag{5.8}$$

b. LJ Potential

For CPCM containing pure PCM and nanoparticles, it is difficult to describe the complicated interactions with a specific potential function. A more general LJ potential energy is usually used to describe the interactions with relative less accuracy, which can be written as follows:

$$U_{\text{non-bond,LJ}}\left(r_{ij}\right)=\begin{cases}4\varepsilon_{ij}\left(\dfrac{\sigma_{ij}^{12}}{r_{ij}^{12}}-\dfrac{\sigma_{ij}^{6}}{r_{ij}^{6}}\right) & r_{ij}<r_{\text{cut}}\\ 0 & r_{ij}\geq r_{\text{cut}}\end{cases} \tag{5.9}$$

where ε, r, and σ represent the well depth (kcal/mol), the distance between atoms (Å) and the characteristic length (Å) for atom i and j, respectively; ε_{ij} and σ_{ij} are all parameters related to atomic types and follow Lorentz–Berthelot mixing rules [29], which are, respectively, determined by:

$$\varepsilon_{ij}=\sqrt{\varepsilon_i\times\varepsilon_j} \tag{5.10}$$

$$\sigma_{ij}=\frac{\sigma_i+\sigma_i}{2} \tag{5.11}$$

5.2.2 Lattice Boltzmann Method

Based on its kinetic characteristics, LBM has been developed as an effective approach to simulate the solid–liquid phase change heat transfer with convenient interface tracking capability. The LBM-based simulation of LHS system could be classified into pore-scale method and REV-scale method [34]. In this section, the pore-scale lattice Boltzmann modeling of solid–liquid phase change conjugate heat transfer is highlighted.

5.2.2.1 Governing Equations for Solid–Liquid Phase Change Conjugate Heat Transfer

The enthalpy-based MRT LBM has already been developed as a major tool for investigating the solid–liquid phase change conjugate heat transfer in the LHS system. The macroscopic governing equation for the solid–liquid phase change heat transfer is given as [65]:

$$\frac{\partial\left(\rho_f h\right)}{\partial t}+\nabla\cdot\left(\rho_f c_{pf}\boldsymbol{u}T_f\right)=\nabla\cdot\left(\lambda_f\nabla T_f\right) \tag{5.12}$$

where ρ_f, c_{pf}, and λ_f are density, specific heat, and thermal conductivity of PCMs, respectively; T_f and $\boldsymbol{u}$ are temperature and fluid flow velocity vector of PCMs, respectively; Besides, t is the time, and the enthalpy h is defined as:

$$h=c_{pf}\left(T_f-T_m\right)+f_l h_{sl} \tag{5.13}$$

where T_m is the melting temperature of PCMs, which is also used as the reference temperature to define the enthalpy value; h_{sl} is the latent heat of PCMs, and f_l is its liquid fraction during melting and solidification. The fluid flow of PCMs at liquid state is governed by the continuity equation and Navier–Stokes equations as:

$$\nabla \cdot \boldsymbol{u} = 0 \tag{5.14}$$

$$\rho_f \left(\frac{\partial \boldsymbol{u}}{\partial t} + \boldsymbol{u} \cdot \nabla \boldsymbol{u} \right) = -\nabla p + \mu \nabla^2 \boldsymbol{u} + \rho_f \boldsymbol{g} \beta \left(T_f - T_m \right) \tag{5.15}$$

where p is the pressure, μ is the dynamic viscosity, g is the gravitational acceleration, and β is the thermal expansion coefficient. Besides, when the extended fins or porous media are inserted into the PCMs to accelerate the heat transfer of LHS system, the corresponding heat conduction occurring inside the solid materials is governed as [66]:

$$\frac{\partial \left(\rho_s c_{ps} T_s \right)}{\partial t} = \nabla \cdot \left(\lambda_s \nabla T_s \right) \tag{5.16}$$

where T_s is the temperature of extended fins or porous media; ρ_s, c_{ps}, and λ_s are density, specific heat, and thermal conductivity of extended fins or porous media, respectively. As aforementioned, conjugate heat transfer occurs at the interface between PCMs and extended fins or porous media, and the Dirichlet–Neumann conditions need to be satisfied in order to guarantee the continuity of heat transfer when the contact thermal resistance is neglected:

$$T_f = T_s \tag{5.17}$$

$$-\lambda_f \nabla T_f = -\lambda_s \nabla T_s \tag{5.18}$$

The governing Eqs. (5.12)–(5.16) in the 2D and 3D Cartesian coordinates could be derived from the Boltzmann equation through Chapman–Enskog expansions. The procedure of solving partial differential equations (PDEs) using LBM includes collision and streaming steps of distribution function, boundary condition tackling, and computation of macroscopic variables. The MRT enthalpy-based LBM for solid–liquid phase change conjugate heat transfer with fluid flow in the 2D and 3D Cartesian coordinates is discussed in this section. Furthermore, the details about MRT enthalpy-based LBM for axisymmetric cylindrical or spherical coordinates could be found in Refs. [40,41].

5.2.2.2 MRT Enthalpy-Based LBM in 2D Cartesian Coordinate

The D2Q9 MRT enthalpy-based LBM is commonly used for simulating solid–liquid phase change conjugate heat transfer in 2D Cartesian coordinate [39]. The evolution equation for the distribution function of total enthalpy h is given by [66]:

$$g_i \left(\boldsymbol{x} + \boldsymbol{e}_i \Delta t, t + \Delta t \right) = g_i \left(\boldsymbol{x}, t \right) - \boldsymbol{M}^{-1} \boldsymbol{S} \left[\boldsymbol{m} \left(\boldsymbol{x}, t \right) - \boldsymbol{m}^{\mathrm{eq}} \left(\boldsymbol{x}, t \right) \right] \tag{5.19}$$

where g_i is the distribution function of enthalpy in velocity space; $\boldsymbol{x}$ is the vector of location on the Cartesian grids; Δt is the time step; $\boldsymbol{e}_i$ is discrete velocity defined by:

$$\boldsymbol{e}_i=\begin{cases}\boldsymbol{e}_0=(0,0)\\ \boldsymbol{e}_i=c\left(\cos\left[(i-1)\pi/2\right],\sin\left[(i-1)\pi/2\right]\right), & i=1,2,3,4\\ \boldsymbol{e}_i=\sqrt{2}c\left(\cos\left[(2i-9)\pi/4\right],\sin\left[(2i-9)\pi/4\right]\right), & i=5,6,7,8\end{cases} \tag{5.20}$$

where c is the lattice speed. $\boldsymbol{m}(\boldsymbol{x},t)$ is the distribution function in momentum space given by:

$$\boldsymbol{m}(\boldsymbol{x},t)=\boldsymbol{M}g_i(\boldsymbol{x},t)=\left(m_0,m_1,m_2,m_3,m_4,m_5,m_6,m_7,m_8\right)^T \tag{5.21}$$

The transformation matrix $\boldsymbol{M}$ is defined as:

$$\boldsymbol{M}=\begin{bmatrix}1&1&1&1&1&1&1&1&1\\-4&-1&-1&-1&-1&2&2&2&2\\4&-2&-2&-2&-2&1&1&1&1\\0&1&0&-1&0&1&-1&-1&1\\0&-2&0&2&0&1&-1&-1&1\\0&0&1&0&-1&1&1&-1&-1\\0&0&-2&0&2&1&1&-1&-1\\0&1&-1&1&-1&0&0&0&0\\0&0&0&0&0&1&-1&1&-1\end{bmatrix} \tag{5.22}$$

Similarly, $\boldsymbol{m}^{\mathrm{eq}}(\boldsymbol{x},t)$ is the equilibrium distribution function in momentum space defined as:

$$\boldsymbol{m}^{\mathrm{eq}}(\boldsymbol{x},t)=\boldsymbol{M}g_i^{\mathrm{eq}}(\boldsymbol{x},t)=\left(m_0^{\mathrm{eq}},m_1^{\mathrm{eq}},m_2^{\mathrm{eq}},m_3^{\mathrm{eq}},m_4^{\mathrm{eq}},m_5^{\mathrm{eq}},m_6^{\mathrm{eq}},m_7^{\mathrm{eq}},m_8^{\mathrm{eq}}\right)^T \tag{5.23}$$

In MRT enthalpy-based LBM for solid–liquid phase change heat transfer, the equilibrium distribution function $\boldsymbol{m}^{\mathrm{eq}}(\boldsymbol{x},t)$ is given by:

$$\boldsymbol{m}^{\mathrm{eq}}\left(\boldsymbol{x},t\right)=\begin{pmatrix}h,-4h+2c_{pf,\mathrm{ref}}T_f+3c_{pf}T_f\dfrac{\boldsymbol{u}^2}{c^2},4h-3c_{pf,\mathrm{ref}}T_f-3c_{pf}T_f\dfrac{\boldsymbol{u}^2}{c^2},\\ c_{pf}T_f\dfrac{u}{c},-c_{pf}T_f\dfrac{u}{c},c_{pf}T_f\dfrac{v}{c},-c_{pf}T_f\dfrac{v}{c},c_{pf}T_f\dfrac{u^2-v^2}{c^2},c_{pf}T_f\dfrac{uv}{c^2}\end{pmatrix}^T \tag{5.24}$$

where $\boldsymbol{u}$ is the vector of fluid flow velocity, and u and v are its distributed velocities in the horizontal x coordinate and vertical y coordinate, respectively. $c_{pf,\,\mathrm{ref}}$ is the reference specific heat, and it is defined by the harmonic mean value of PCM specific heat c_{pf} and solid material specific heat c_{ps} to satisfy the Dirichlet–Neumann conditions of Eqs. (5.17) and (5.18) for conjugate heat transfer at PCM-solid material interface:

$$c_{pf,\,\mathrm{ref}} = \frac{2c_{pf}c_{ps}}{c_{pf} + c_{ps}} \tag{5.25}$$

Specifically, the relaxation matrix $\boldsymbol{S}$ in momentum space is given as:

$$\boldsymbol{S} = \mathrm{diag}\left(s_0, s_e, s_\varepsilon, s_j, s_q, s_j, s_q, s_e, s_e\right) \tag{5.26}$$

The relaxation parameters in the diagonal matrix $\boldsymbol{S}$ should satisfy the following relation:

$$s_0 = 1,\ s_j = 1/\tau_T,\ \text{and}\ 0 < s_{e,\varepsilon,q} < 2 \tag{5.27}$$

where τ_T is the relaxation time of enthalpy distribution function:

$$\tau_T = \begin{cases} 3\dfrac{\lambda_f}{\rho_{\mathrm{ref}} c_{p,\,\mathrm{ref}}} + 0.5, & \text{PCMs} \\ 3\dfrac{\lambda_s}{\rho_{\mathrm{ref}} c_{p,\,\mathrm{ref}}} + 0.5, & \text{Solid materials} \end{cases} \tag{5.28}$$

where ρ_{ref} is a harmonic mean value of PCM density ρ_f and density of solid materials ρ_s. Besides, to reduce the numerical diffusion during solid–liquid phase change heat transfer, the relaxation parameters should also be kept as [39]:

$$\left(\frac{1}{s_e} - \frac{1}{2}\right)\left(\frac{1}{s_j} - \frac{1}{2}\right) = \frac{1}{4} \tag{5.29}$$

The collision step for enthalpy distribution function is completed in momentum space as:

$$\boldsymbol{m}\left(\boldsymbol{x}, t + \Delta t\right) = \boldsymbol{m}\left(\boldsymbol{x}, t\right) - \boldsymbol{S}\left[\boldsymbol{m}\left(\boldsymbol{x}, t\right) - \boldsymbol{m}^{\mathrm{eq}}\left(\boldsymbol{x}, t\right)\right] \tag{5.30}$$

The post-collision distribution function in velocity space is inversely transformed as:

$$g_i\left(\boldsymbol{x}, t + \Delta t\right) = \boldsymbol{M}^{-1}\boldsymbol{m}\left(\boldsymbol{x}, t + \Delta t\right) \tag{5.31}$$

Then, the streaming process is handled as:

$$g_i\left(\boldsymbol{x}+\boldsymbol{e}_i\Delta t, t+\Delta t\right)=g_i\left(\boldsymbol{x}, t+\Delta t\right) \tag{5.32}$$

After handling the thermal boundary conditions with different numerical schemes [67–69], the macroscopic enthalpy h could be computed as:

$$h=\sum_i g_i \tag{5.33}$$

The transient liquid fraction f_l of PCMs could be calculated as:

$$f_l=\begin{cases}0,\ h\le h_s\\ \dfrac{h-h_s}{h_l-h_s},\ h_s<h<h_l\\ 1,\ h\ge h_l\end{cases} \tag{5.34}$$

The corresponding temperature T_f of PCMs could be further given as:

$$T_f=\begin{cases}T_m-\dfrac{h_s-h}{c_{pf}},\ h\le h_s\\ T_m,\ h_s<h<h_l\\ T_m-\dfrac{h-h_l}{c_{pf}},\ h\ge h_l\end{cases} \tag{5.35}$$

Besides, the temperature T_s of solid materials is computed by:

$$T_s=\frac{h}{c_{ps}}+T_m \tag{5.36}$$

To simulate the convective heat transfer caused by fluid flow, the details about 2D MRT LBM for incompressible flow could be found in Refs. [70,71].

5.2.2.3 MRT Enthalpy-Based LBM in 3D Cartesian Coordinate

The D3Q7 MRT enthalpy-based LBM is derived for simulating solid–liquid phase change conjugate heat transfer in the 3D Cartesian coordinate [42]. Similarly, the collision step of enthalpy distribution function is also carried out in momentum space as presented in Eq. (5.30). For D3Q7 MRT enthalpy-based LBM, the enthalpy distribution function $\boldsymbol{m}$ in momentum space and its corresponding transformation matrix $\boldsymbol{M}$ are defined as:

$$\boldsymbol{m}\left(\boldsymbol{x}, t\right) = \boldsymbol{M}\left(g_0, g_1, g_2, g_3, g_4, g_5, g_6\right)^T \tag{5.37}$$

$$\boldsymbol{M} = \begin{bmatrix} 1 & 1 & 1 & 1 & 1 & 1 & 1 \\ 0 & 1 & -1 & 0 & 0 & 0 & 0 \\ 0 & 0 & 0 & 1 & -1 & 0 & 0 \\ 0 & 0 & 0 & 0 & 0 & 1 & -1 \\ 6 & -1 & -1 & -1 & -1 & -1 & -1 \\ 0 & 2 & 2 & -1 & -1 & -1 & -1 \\ 0 & 0 & 0 & 1 & 1 & -1 & -1 \end{bmatrix} \tag{5.38}$$

The equilibrium distribution function $\boldsymbol{m}^{\mathrm{eq}}\left(\boldsymbol{x},t\right)$ is given as:

$$\boldsymbol{m}^{\mathrm{eq}}\left(\boldsymbol{x}, t\right) = \left(h, \frac{c_{pf}T_f u_x}{c}, \frac{c_{pf}T_f u_y}{c}, \frac{c_{pf}T_f u_z}{c}, 6h - 21\omega_T c_{pf,\,\mathrm{ref}} T_f, 0, 0\right)^T \tag{5.39}$$

where u_x, u_y, and u_z are respectively the velocities in three orthogonal directions of Cartesian coordinate; ω_T is a constant set to be 0.25 in this model, and $c_{pf,\,\mathrm{ref}}$ is the reference specific heat defined by the harmonic mean value of PCM specific heat c_{pf} and solid material specific heat c_{ps} as presented in Eq. (5.25). In addition, the relaxation matrix $\boldsymbol{S}$ in momentum space for D3Q7 MRT enthalpy-based LBM is:

$$\boldsymbol{S} = \mathrm{diag}\left(\sigma_0, \sigma_1, \sigma_2, \sigma_3, \sigma_4, \sigma_5, \sigma_6\right) \tag{5.40}$$

The relaxation parameters in the diagonal matrix $\boldsymbol{S}$ should satisfy the following relation to reduce the numerical diffusion during solid–liquid phase change:

$$\sigma_0 = 1,\ \sigma_1 = \sigma_2 = \sigma_3 = \frac{1}{\tau_T},\ \sigma_4 = \sigma_5 = \sigma_6 = 2 - \frac{1}{\tau_T} \tag{5.41}$$

The relaxation time τ_T of enthalpy distribution function in D3Q7 model is given as:

$$\tau_T = \begin{cases} 4\dfrac{\lambda_f}{\rho_{\mathrm{ref}} c_{p,\,\mathrm{ref}}} + 0.5, & \text{PCMs} \\ 4\dfrac{\lambda_s}{\rho_{\mathrm{ref}} c_{p,\,\mathrm{ref}}} + 0.5, & \text{Solid materials} \end{cases} \tag{5.42}$$

Similarly as the 2D MRT enthalpy-based LBM for solid–liquid phase change conjugate heat transfer, the macroscopic enthalpy h could be achieved by Eq. (5.33) after the streaming of post-collision distribution functions in velocity space and tackling the boundary conditions using appropriate numerical schemes. Then, the liquid fraction of PCM f_l, PCM temperature T_f, and solid material temperature T_s is further calculated according to Eqs. (5.34)–(5.36), respectively.

5.2.2.4 Numerical Reconstruction of Porous Media

High thermal conductive porous media are widely inserted into the LHS system to ameliorate its thermal response during charging and discharging processes because of their interconnected heat transfer channels. A significant advantage of MRT enthalpy-based LBM is its powerful capability in pore-scale modeling of the solid–liquid phase change conjugate heat transfer in porous medium enhanced LHS system. Under this circumstance, numerical methodologies for reconstructing porous medium morphology become essential for accurately simulating the melting and solidification behaviors. The quartet structure generation set (QSGS) is a famous approach to numerically reconstruct the porous foam geometries [72]. The metal foam-PCM composite is effectively reconstructed using QSGS as displayed in Figure 5.1 with respect to different porosity and pore size, and its reconstruction procedure is as follows [14]: (1) Randomly locate the center of a pore in the domain and expand it into the neighboring cells until reaching to the pore diameter $\left(d = d_p \pm 0.2d_p\right)$, where d is the reconstructed pore diameter and d_p is the average pore diameter. (2) Repeat the growing step 1 for other pores and the region of different pores could be overlapped. (3) Stop the growing process if the total area fraction of the pores reaches to $\left(1-\varepsilon_{\text{ave}}\right)\pm 0.001$, where ε_{ave} is the average porosity of metal foams. (4) To reconstruct the metal foam with non-uniform porosity, steps 1–3 are used to generate five different layers with porosity $\left(\varepsilon = \varepsilon_{\text{ave}} \pm 0.02, 0.04\right)$, respectively.

Besides the porous foams, porous fibers are also promising for enhancing the heat transfer performance in the LHS system due to their flexibility in modulating the consolidated heat transfer directions. The random generation-growth method is generally used to reconstruct the morphology of metal fibers [73,74]. Specifically, the growth direction possibility of woven metal fibers follows the Gaussian distribution as [75]:

$$F_g(\theta) = \frac{1}{\sqrt{2\pi}}\exp\left[-\frac{(\theta-\theta_0)^2}{2\sigma_d^2}\right] \tag{5.43}$$

where θ_0 is the major growth direction of woven fibers, and σ_d is the distribution standard deviation of fiber growth direction which indicates the anisotropic degree of woven fibers. As shown in Figure 5.2, the woven metal fibers with different diameter,

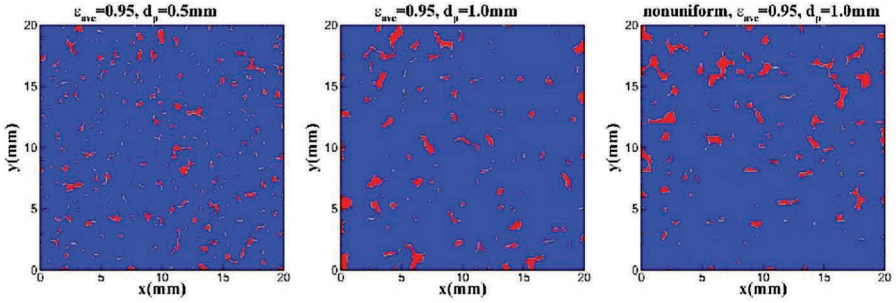

FIGURE 5.1 Reconstructed metal foams using QSGS [14].

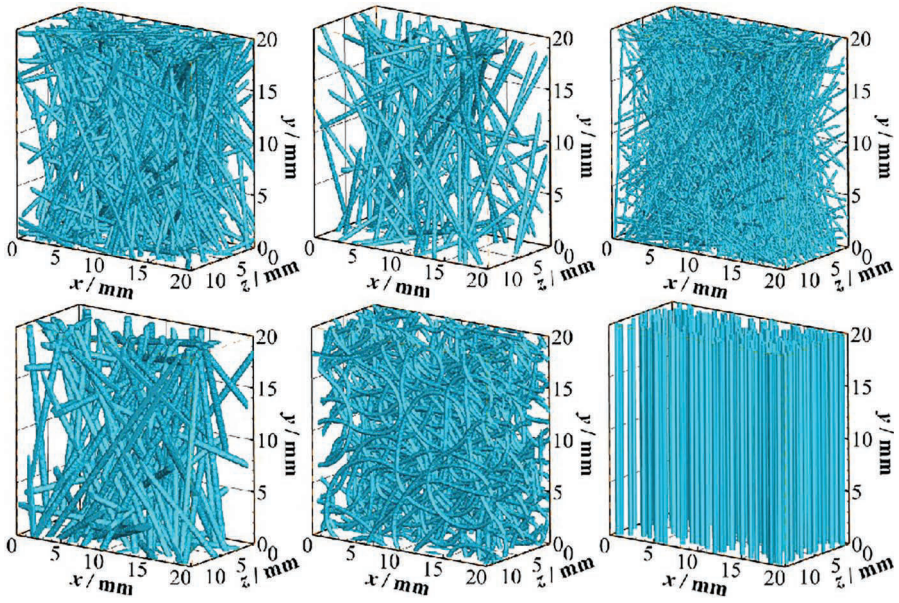

FIGURE 5.2 Reconstructed woven fibers with different diameter, porosity, curvature, and anisotropic degree [75].

porosity, curvature, and anisotropic degree are successfully reconstructed using the random generation-growth method [75].

5.2.2.5 Graphic Processor Units (GPUs) Computing

Based on the rapid hardware development of GPUs, GPU computing becomes attractive during the past decade due to its fantastic capability for tackling parallel modeling task. Due to its highly parallel kinetic nature, LBM has been successfully fitted onto GPUs to efficiently simulate several heat transfer and fluid flow problems on a CUDA programming platform [76–78]. During GPU computing, the CPU and GPUs work as host and devices, respectively. The sequential time steps and initial conditions of LBM are executed on CPU, while GPUs are responsible for all the parallel tasks [79]. Firstly, the initial conditions are set up in host memory and then move the data to the memory of GPUs. A kernel is a function executed in the concurrent threads on GPUs. When the kernels are started for LBM simulation, the collision and streaming steps of distribution functions, tackling of boundary conditions, and computing the macroscopic variables at different lattice grids are simultaneously carried out. Significantly, the kernels need to be synchronized between CPU and GPUs to guarantee the computational logic of LBM. Finally, the data achieved on the threads of GPUs needs to be moved back to the host memory on CPU for further printing out. To test the acceleration ratio on LBM computational speed using GPUs, the unidirectional flow in a 3D microfluidic channel is simulated by LBM, and the parallel acceleration of GPU computing is presented in Table 5.1 [80]. When the Quadro GV 100 type GPU

TABLE 5.1
Computational Acceleration of GPU-Based LBM

Lattice Grid Numbers	100 * 100 * 100	150 * 150 * 150	200 * 200 * 200
CPU intel core i7 8770 s/LBM time step	10.742	34.525	83.174
GPU Quadro GV 100 s/LBM time step	0.025	0.0664	0.1493
Acceleration ratio	429.68	519.95	557.09

is used for parallel computing, the LBM computation could be accelerated by 557.09 times at a grid number of $200 \times 200 \times 200$ in comparison to serial CPU LBM code.

5.2.3 Finite Volume Method

When FVM is used to simulate the solid–liquid phase change heat transfer inside the LHS system, the enthalpy-based energy equation as shown in Eq. (5.12) is transformed into a temperature-based energy equation with a latent heat source term as:

$$\frac{\partial\left(\rho_f T_f\right)}{\partial t} + \nabla \cdot \left(\rho_f \boldsymbol{u} T_f\right) = \nabla \cdot \left(\frac{\lambda_f}{c_{pf}} \nabla T_f\right) - \frac{\rho_f h_{sl}}{c_{pf}} \frac{\partial f_l}{\partial t} \tag{5.44}$$

Therefore, the continuity equation of Eq. (5.14), momentum equation of Eq. (5.15), and energy equation of Eq. (5.44) are simultaneously solved, and they could be expressed by the following general governing equations:

$$\begin{aligned} &\frac{\partial(\rho_f \phi)}{\partial t} + \frac{\partial(\rho_f u_x \phi)}{\partial x} + \frac{\partial(\rho_f u_y \phi)}{\partial y} + \frac{\partial(\rho_f u_z \phi)}{\partial y} \\ &= \frac{\partial}{\partial x}\left(\Gamma_\phi \frac{\partial \phi}{\partial x}\right) + \frac{\partial}{\partial y}\left(\Gamma_\phi \frac{\partial \phi}{\partial y}\right) + \frac{\partial}{\partial z}\left(\Gamma_\phi \frac{\partial \phi}{\partial z}\right) + S_\phi \end{aligned} \tag{5.45}$$

where ϕ is a general variable representing PCM temperature T_f and fluid flow velocities u_x, u_y, and u_z. The general diffusion coefficient Γ_ϕ and source term S_ϕ for continuity equation, momentum equation, and energy equation are summarized in Table 5.2.

Based on the FVM with integration over each control volumes, the general governing equation for solid–liquid phase change heat transfer in 2D Cartesian coordinate could be discretized into the following linear system of equations using IDEAL algorithm [54]:

$$a_P \phi_P = a_E \phi_E + a_W \phi_W + a_N \phi_N + a_S \phi_S + b \tag{5.46}$$

TABLE 5.2
Expression of General Diffusion Coefficient and Source Term in Various Governing Equations

Governing equations	ϕ	Γ_ϕ	S_ϕ
Continuity equation	1	0	0
Momentum equation	$\boldsymbol{u}$	μ	$-\nabla p + \rho_f \boldsymbol{g}\beta\left(T_f - T_m\right)$
Energy equation	T_f	$\frac{\lambda_f}{c_{pf}}$	$-\frac{\rho_f h_{sl}}{c_{pf}}\frac{\partial f_l}{\partial t}$

where coefficients a_E, a_W, a_N, a_S, a_P, and source term b are given as:

$$a_E = D_e A(P_{\Delta e}) = D_e A\left(\left|P_{\Delta e}\right|\right) + \left[\left| - F_e,\ 0\right|\right] \tag{5.47}$$

$$a_W = D_w A(P_{\Delta w}) = D_w A\left(\left|P_{\Delta w}\right|\right) + \left[\left| - F_w,\ 0\right|\right] \tag{5.48}$$

$$a_N = D_n A(P_{\Delta n}) = D_n A\left(\left|P_{\Delta n}\right|\right) + \left[\left| - F_n,\ 0\right|\right] \tag{5.49}$$

$$a_S = D_s A(P_{\Delta s}) = D_s A\left(\left|P_{\Delta s}\right|\right) + \left[\left| - F_s,\ 0\right|\right] \tag{5.50}$$

$$b = S_c \Delta V + a_p{}^0 \phi_p{}^0 \tag{5.51}$$

$$a_P = a_E + a_W + a_N + a_S - S_p \Delta V \tag{5.52}$$

$$a_P{}^0 = \frac{\rho_P \Delta V}{\Delta t} \tag{5.53}$$

The detail information of parametric coefficients in Eqs. (5.46)–(5.53) could be found in the Ref. [52]. Besides, several other FVM schemes using combined VOF and level-set approach (VOSET) or phase-field method are also developed for solid–liquid phase change heat transfer in the LHS system as presented in Refs. [56,81].

5.2.4 LBM-FVM Coupling Schemes

The coupling schemes of LBM-FVM are essential for carrying out multi-scale numerical modeling of heat transfer and fluid flow with economic computational load. In the multi-scale simulation method called "solving problems regionally and coupling at the interfaces", the computational domain is divided into several sub-regions and

different numerical methods (or models) are used to simultaneously simulate transport processes in different sub-regions, while the information in different regions is exchanged at their interfaces as shown in Figure 5.3. Based on this, Chen et al. derived the expressions of LBM density distribution functions up to second order from the macroscopic velocity and density using Champan–Enskog expansion [21], and they apply the coupling simulation strategy using FVM and LBM to more complicated fluid flow. Furthermore, they also derived the expressions of LBM temperature (concentration) distribution functions up to second order from the macroscopic temperature (concentration) using Champan–Enskog expansion, and they applied the coupling simulation strategy to convective heat (species) transfer processes [82].

Besides, a general expression of the density distribution functions up to second order for any scalar that obeys the convective-diffusion (CD) equation is also proposed. For fluid flow usually encountered, the Chapman–Enskog multi-scale expansion technique is used to derive the distribution function up to $f(2)$, which is expressed as follows together with $f(0)$ and $f(1)$:

$$f_i^{(0)} = f_i^{(\mathrm{eq})} \tag{5.54}$$

$$f_i^{(1)} = -\tau_f \Delta t (c_{i\alpha} - u_\alpha)(c_{i\beta} - u_\beta) f_i^{(0)} c_s^{-2} \partial_{x_\alpha}^{(1)} u_\beta \tag{5.55}$$

$$f_i^{(2)} = -\Delta t \tau_f \upsilon (c_{i\beta} - u_\beta) f_i^{(0)} c_s^{-2} \left[\frac{1}{\rho} (\partial_{x_\beta}^{(1)} u_\alpha + \partial_{x_\alpha}^{(1)} u_\beta) \partial_{x_\alpha}^{(1)} \rho + \left(\partial_{x_\alpha}^{(1)} \right)^2 u_\beta \right] \tag{5.56}$$

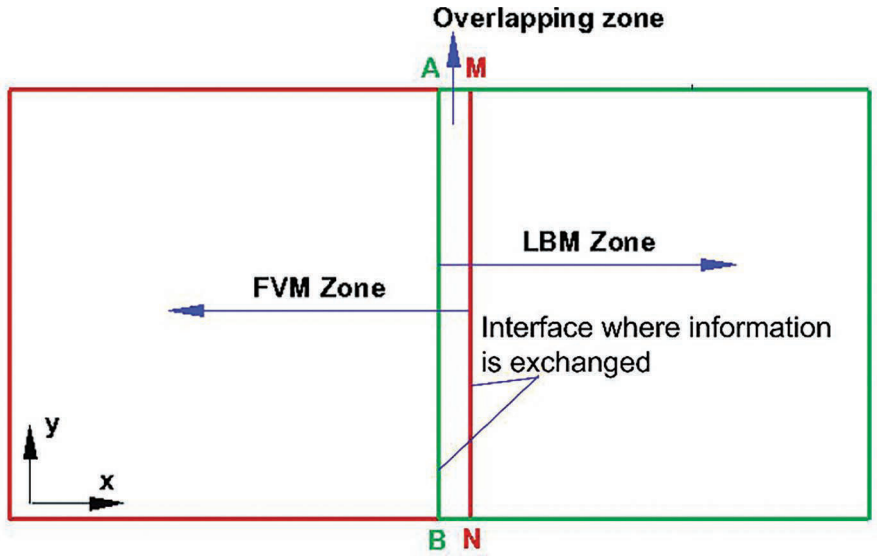

FIGURE 5.3 FVM–LBM coupled computational domain: One region is simulated using FVM and the other is simulated using LBM. Information is exchanged at their interfaces.

where $f_i^{(1)}$ and $f_i^{(2)}$ refer to the first-order and second-order distribution functions. Δt, τ_f, c, c_s are the time step, relaxation time, lattice speed, and sound speed in the LBM, respectively. The detail of the deriving process could be found in Ref. [83,84]. Several typical fluid flow problems are simulated including backward-facing step flow, flow around a circular cylinder, and lid-driven cavity flow [83,84] using the MRCA-DMDV, namely multi (M) regions (R) coupling (C) approach (A)–different (D) numerical methods (M) with different (D) basic variables (V), and good agreements are obtained between the coupling simulation results and numerical results in literature. For heat transfer or mass transport, the following distribution functions based on the Chapman–Enskog expansion $g(0)$, $g(1)$, and $g(2)$ are given:

$$g_i^{(0)} = g_i^{\mathrm{eq}} \tag{5.57}$$

$$g_i^{(1)} = -\tau_g \Delta t \left[(c_{i\alpha} - u_\alpha) C^{-1} g_i^{(eq)} \partial_{x_\alpha}^{(1)} C + 0.5 (c_{i\alpha} - u_\alpha) C c_{i\beta} \partial_{x_\alpha}^{(1)} u_\beta - 0.5 \rho^{-1} C c_{i\beta} \partial_{x\beta}^{(1)} \rho \right] \tag{5.58}$$

$$g_i^{(2)} = -\tau_g \Delta t \left[D C^{-1} g_i^{(eq)} \partial_{x_\alpha}^{(1)} \partial_{x_\alpha}^{(1)} C + 0.5 C c_{i\beta} \rho^{-1} \nu \left[\rho \partial_{x_\alpha}^{(1)} \partial_{x_\alpha}^{(1)} u_\beta + (\partial_{x_\beta}^{(1)} u_\alpha + \partial_{x_\alpha}^{(1)} u_\beta) \partial_{x_\alpha}^{(1)} \rho \right] \right] \tag{5.59}$$

where τ_g is the relaxation time for temperature (concentration) distribution function. The detailed derivation can be found in Ref. [21]. The MRCA-DMDV is applied to simulate several typical convective-diffusion-reaction problems including species convection and diffusion in a rectangular domain with bulk reaction, species diffusion in a rectangular domain with reaction on the top boundary, fluid flow and mass transport processes in fuel cells, as well as coupled fluid flow, heat and mass transfer, and reaction in microreactors [21,82].

5.3 APPLICATIONS OF MULTI-SCALE MODELING TO LATENT HEAT THERMAL ENERGY STORAGE

Based on the advantages of multi-scale numerical methods for analyzing solid–liquid phase change conjugate heat transfer, the thermal response behavior of latent heat TES system with diverse heat transfer enhancement technologies is widely simulated and optimized during recent years. In this section, we firstly focus on the thermophysical properties of PCMs computed through MD simulation, which actually offers the foundation for mesoscopic and macroscopic modeling of solid–liquid phase change heat transfer. Due to its effectiveness in handling transport phenomenon in porous media with complex boundary geometries, pore-scale lattice Boltzmann modeling for solid–liquid phase change conjugate heat transfer in the LHS system is further reviewed. Finally, the macroscopic FVM for investigating the thermal behavior of LHS system is also discussed to promote practical engineering applications.

5.3.1 Thermophysical Properties of PCMs

MD simulations are successfully used to calculate several thermophysical properties of PCMs including thermal conductivity, specific heat, melting enthalpy, melting point, density, and thermal expansion coefficients, which serve as significant supplements for experimental measurements. In this section, we mainly focus on the MD simulations for specific heat and melting enthalpy of PCMs because these parameters significantly influence the charging and discharging processes of LHS system.

5.3.1.1 Specific Heat Capacity and Melting Enthalpy

The specific heat capacity determines the sensible heat storage density and melting enthalpy determines the latent heat storage density of PCMs, which are significant for thermal performance of LHS system. To calculate the specific heat capacity and melting enthalpy using MD simulation, PCM is heated from solid state to liquid state in NPT ensemble, and the corresponding energy, volume, and temperature are recorded. Then, the specific heat capacity and melting enthalpy can be obtained [85]:

$$c_p = \left(\frac{\partial H}{\partial T} \right)_P = \frac{1}{k_B T^2} \left\langle \delta \left(E_K + U + pV \right)^2 \right\rangle \approx \frac{\Delta H}{\Delta T \cdot \rho \cdot V} \tag{5.60}$$

where H is the total enthalpy of the system (kJ/mol); k_B is the Boltzmann constant, and E_K and U are the kinetic energy (kJ/mol) and the potential energy (kJ/mol) of the system, respectively. p, V, and T are the pressure (Pa), volume (m^3), and temperature (K) of the system, respectively. The melting enthalpy ΔH is defined as the difference of the total enthalpy of PCMs during the phase transition (J/g). As displayed in Figure 5.4, the specific heat c_p and melting enthalpy ΔH for NaCl-single walled carbon nanotube (SWCNT) composite are achieved by MD simulation with respect to different mass fraction of SWCNT [29]. The results indicate that the specific heat capacity c_p is enhanced with an increased mass fraction of SWCNT, while the corresponding melting enthalpy ΔH is attenuated.

5.3.2 Pore-Scale Modeling of LHS System

Based on the MRT enthalpy-based LBM for solid–liquid phase change conjugate heat transfer, pore-scale investigation of thermal behavior in porous medium-PCM composite is carried out. Under this circumstance, the morphology of porous media could be further optimized to improve the latent heat TES performance. Ren et al. presented a pore-scale investigation of melting process in a latent heat TES unit filled with metal foams by pore-scale lattice Boltzmann modeling under GPU acceleration [14]. The QSGS method is used to reconstruct the diversified morphology of metal foams. As shown in Figure 5.5, at a specific porosity of metal foams, the melting rate of PCMs is accelerated with a decreased pore size due to the enhanced specific surface area of metal foams, which also makes the temperature distribution inside LHS unit more uniform. In addition, due to the trade-off effect between increasing the heat transfer rate by using metal foam with lower porosity and the reduced amount of

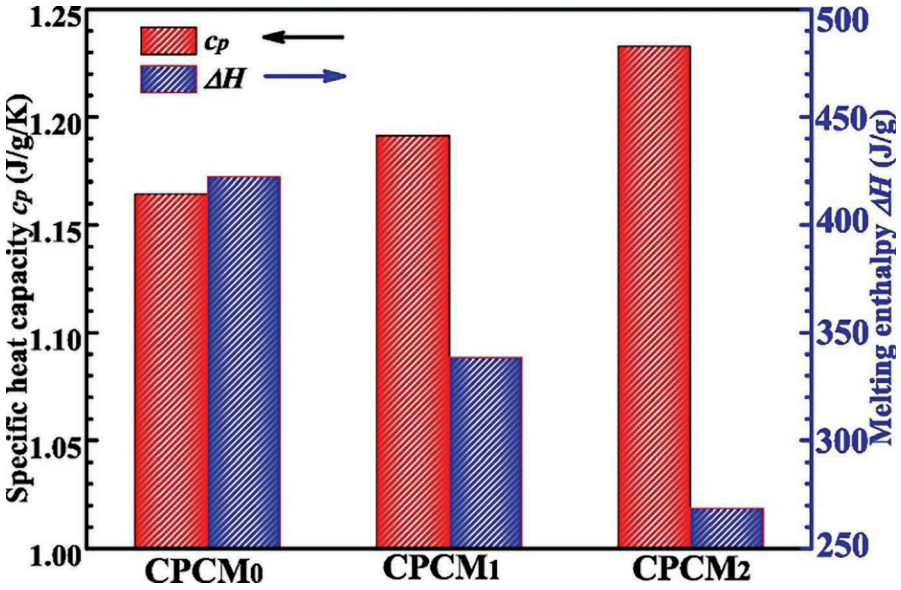

FIGURE 5.4 The melting enthalpy ΔH and specific heat capacity c_p of NaCl-SWCNT.

energy stored in the LHS unit, an appropriate metal foam porosity is highly recommended in the practical engineering applications to balance the charging and discharging rates and energy storage capacity.

To achieve a deep understanding for solid–liquid phase change conjugate heat transfer in the LHS unit, a 3D pore-scale lattice Boltzmann modeling is necessary. Recently, Ren et al. investigated the charging process of woven metal fiber-PCM composite at pore-scale by numerically reconstructing the various morphologies of metal fibers with respect to fiber porosity, fiber diameter, fiber curvature, and the anisotropic degree of fibers [75]. As displayed in Figure 5.6, the energy storage rate in a LHS unit could be accelerated by 40% through consolidating the anisotropic degree of woven metal fibers from $\sigma = 0.5$ to $\sigma = 0$ because of the enhanced heat transfer capability in a desired vertical direction. Similarly, woven metal fibers with appropriate porosity need to be used in order to balance the heat conduction rate inside fiber skeleton and the energy storage capacity of LHS unit. In addition, the heat conduction inside metal fiber-PCM composite is observed to be consistently dominant over natural convection even though the role of natural convection is consolidated with the increment of fiber porosity or characteristic temperature difference.

The aforementioned researches demonstrate the effectiveness of investigating solid–liquid phase change conjugate heat transfer in the LHS unit using pore-scale lattice Boltzmann modeling, which contributes to improving heat transfer enhancement technologies for optimizing the energy storage rate and energy storage capacity of LHS system.

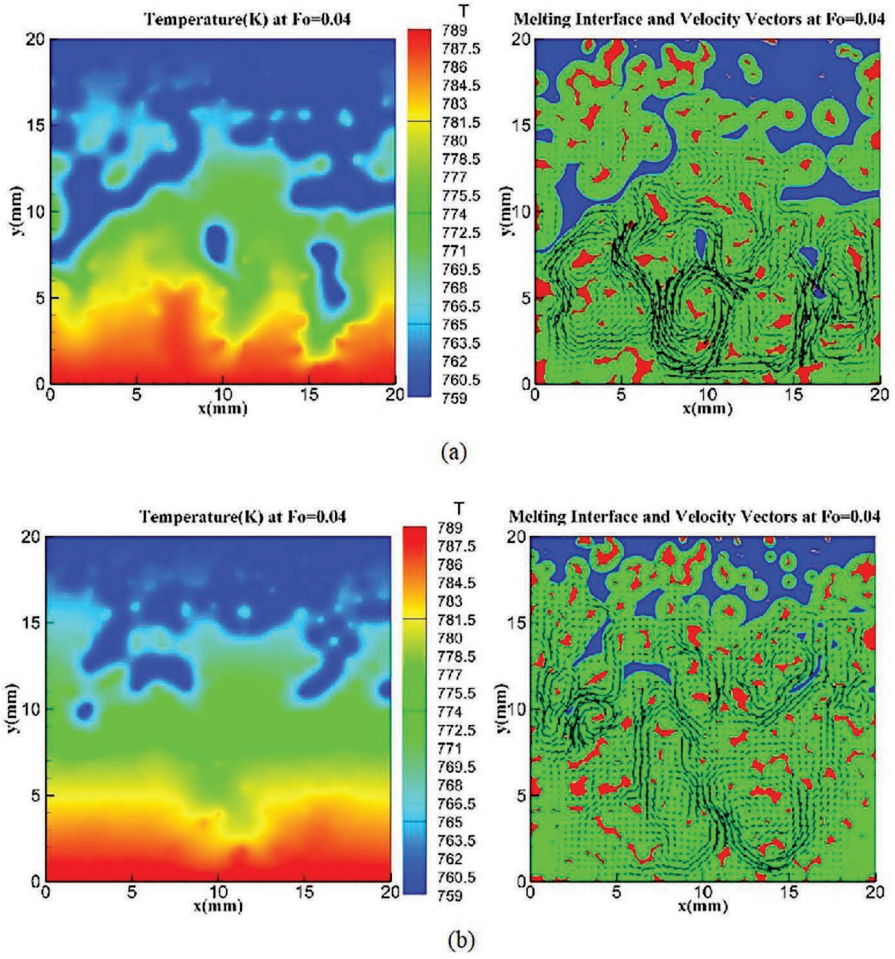

FIGURE 5.5 Melting process of porous medium-PCM composite at heat temperature $T_h = 789\ K$, initial temperature $T_c = 759\ K$, porosity $\varepsilon_{ave} = 0.95$ at different pore size d_p (a) $d_p = 1$ mm (b) $d_p = 0.75$ mm.

5.3.3 Representative Elementary Volume Scale Modeling of LHS System

The numerical modeling of solid–liquid phase change conjugate heat transfer at REV scale is significant for optimizing the thermal behavior of integrated LHS systems in engineering applications due to the relatively high computational efficiency compared with mesoscopic lattice Boltzmann modeling. Li et al. numerically investigated the open-cell metallic foams filled with paraffin at REV scale using FVM with consideration of the non-Darcy effect, local natural convection, and thermal non-equilibrium [55]. As shown in Figure 5.7, the numerical simulation using FVM at REV scale for solid–liquid phase change heat transfer in metal foam-PCM composite is consistent with the experimental results, which validates the accuracy of numerical

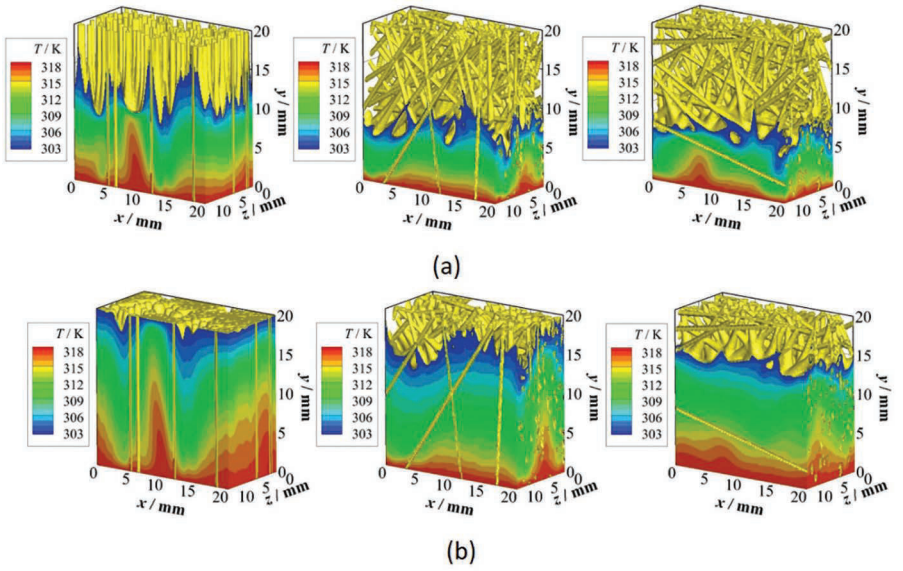

FIGURE 5.6 Solid–liquid phase change process of anisotropic straight woven metal fiber-PCM composite at porosity $\varepsilon = 0.90$, diameter $D = 0.4$ mm, and temperature difference $\Delta T = 15$K for different fiber anisotropic degree (a) From left to right: anisotropic degree $\sigma = 0$, $\sigma = 0.25$, and $\sigma = 0.50$ at time $t = 124.2$ s (b) From left to right: anisotropic degree $\sigma = 0$, $\sigma = 0.25$, and $\sigma = 0.50$ at time $t = 372.6$ s.

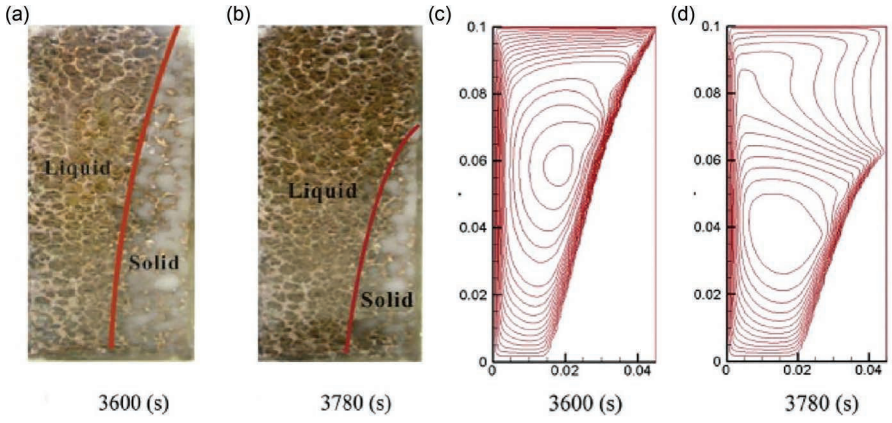

FIGURE 5.7 Comparison of the solid–liquid interface between the experimental photos and REV-scale numerical results at different times for metal foam at $\varepsilon = 0.90$, $\omega = 10$ PPI (a) Experimental photo at time $t = 3600$ s (b) Experimental photo at time $t = 3780$ s (c) Numerical results at time $t = 3600$ s (d) Numerical results at time $t = 3780$ s.

modeling in designing LHS system. Their results also indicate that the melting heat transfer is enhanced by the high thermal conductivity matrix foams even though the local natural convection is suppressed to some extent.

Furthermore, the commercial software ANSYS FLUENT based on FVM with SIMPLE algorithm is popular used by several researchers to investigate the solid–liquid phase change in LHS system with different heat transfer enhancement technologies at REV scale. For instance, Xu et al. applied ANSYS FLUENT to numerically investigate the melting performance of triplex-layer PCMs in a horizontal shell and tube LHS unit [86]. As shown in Figure 5.8, the transient melting process of LHS unit is analyzed with respect to different fin arrangements. The results show that the uniform radial fin arrangement in each PCM layers presents the maximum value of comprehensive storage density evaluation (CSDE), which is a significant criterion to evaluate the performance of LHS system. A large amount of research results for the thermal behavior of LHS system using FVM-based ANSYS FLUENT can be found in review Refs. [53,87].

5.4 CONCLUSIONS

Multi-scale numerical modeling is an effective tool for investigating solid–liquid phase change conjugate heat transfer in the latent heat TES applications. In this chapter, the multi-scale numerical methods including molecular dynamics simulation, LBM, and FVM for simulating thermal behavior of latent heat unit are systematically discussed with classical examples. Specifically, the molecular dynamics simulation is powerful

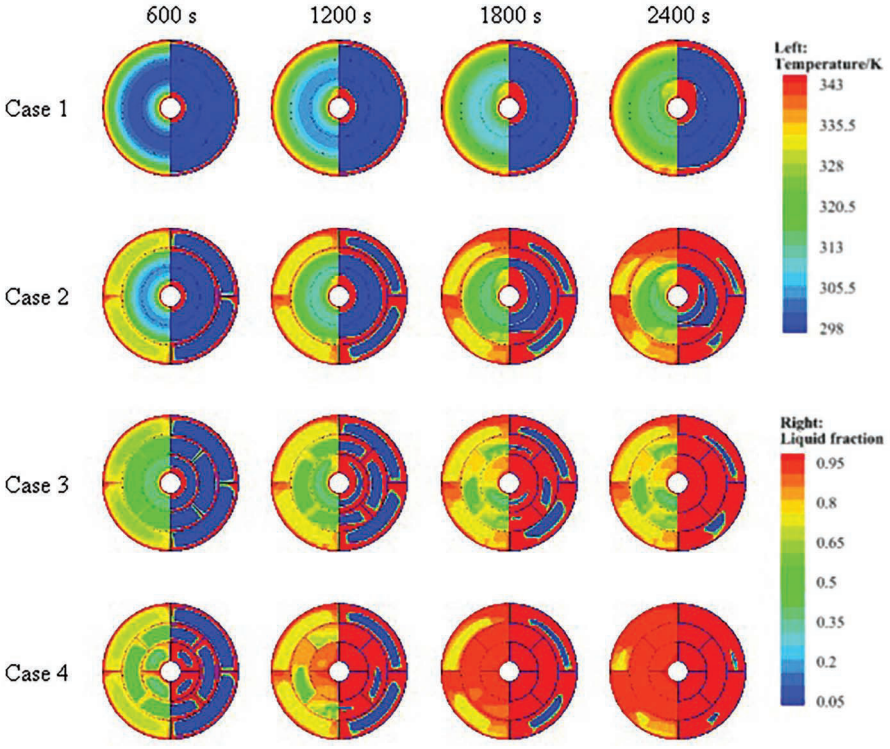

FIGURE 5.8 Temperature (left) and liquid fraction (right) contours with respect to time for different fin arrangements.

for computing the thermophysical properties of PCMs, laying foundations for mesoscopic and macroscopic numerical simulations. In addition, due to its kinetic nature, LBM is efficient for clarifying the heat transfer and fluid flow in porous medium-PCM composite at pore-scale due to its outstanding ability for handling complicated boundary conditions. Besides, as a traditional numerical method developed for more than 50 years, FVM is robust on simulating the macroscopic thermal performance of LHS system at REV scale. Based on the advantages of various numerical methods at different scales with their coupling scheme, multi-scale numerical modeling contributes to several research achievements in designing fantastic latent heat TES systems. With the rapid progress of numerical methods and computational hardware such as GPUs, the multi-scale modeling will definitely play an increasing role in optimizing practical latent heat TES applications in recent future.

ACKNOWLEDGMENTS

This work is supported by the project of the National Natural Science Foundation of China (No. 51806168), and the Foundation for Innovative Research Groups of the National Natural Science Foundation of China (No. 51721004).

REFERENCES

1. Guruprasad Alva, Yaxue Lin, Guiyin Fang, An overview of thermal energy storage systems, *Energy* 144 (2018) 341–378.
2. Atul Sharma, V. Veer Tyagi, Carl R. Chen, Dharam Buddhi, Review on thermal energy storage with phase change materials and applications, *Renewable and Sustainable Energy Reviews* 13 (2009) 318–345.
3. Francis Agyenim, Neil Hewitt, Philip Eames, Mervyn Smyth, A review of materials, heat transfer and phase change problem formulation for latent heat thermal energy storage systems (LHTESS), *Renewable and Sustainable Energy Reviews* 14 (2) (2010) 615–628.
4. Nasiru I. Ibrahim, Fahad A. Al-Sulaiman, Saidur Rahman, Bekir S. Yilbas, Ahmet Z. Sahin, Heat transfer enhancement of phase change materials for thermal energy storage applications: A critical review, *Renewable and Sustainable Energy Reviews* 74 (2017) 26–50.
5. Yaxue Lin, Yuting Jia, Guruprasad Alva, Guiyin Fang, Review on thermal conductivity enhancement, thermal properties and applications of phase change materials in thermal energy storage, *Renewable and Sustainable Energy Reviews*. 82 (2018) 2730–2742.
6. Kin Yuen Leong, Mohd Rosdzimin Abdul Rahman, Balamurugan A. Gurunathan, Nano-enhanced phase change materials: A review of thermo-physical properties, applications, and challenges, *Journal of Energy Storage* 21 (2019) 18–31.
7. Jianjian Wang, Ruiting Zheng, Jinwei Gao, Gang Chen, Heat conduction mechanisms in nanofluids and suspensions, *Nano Today* 7 (2) (2012) 124–136.
8. Syeda Laraib Tariq, Hafiz Muhammad Ali, Muhammad Ammar Akram, Muhammad Mansoor Janjua, Majid Ahmadlouydarab, Nanoparticle enhanced phase change materials (NePCMs) – A recent review, *Applied Thermal Engineering* 176 (2020) 115305.
9. Srikanth Salyan, S. Suresh, Study of the thermos-physical properties and cycling stability of D-Mannitol-copper oxide nanocomposites as phase change materials, *Journal of Energy Storage* 15 (2018) 245–255.
10. Ammar M. Abdulateef, Sohif Mat, Jasim Abdulateef, Kamaruzzaman Sopian, Abduljalil A. Al-Abidi, Geometric and design parameters for fins employed for enhancing thermal energy storage systems: A review, *Sustainable Energy Reviews* 82 (1) (2018) 1620–1635.

11. J.P. Holman, *Heat Transfer*, 10th ed. New York: MCGraw-Hill Companies, 2010.
12. Shuai Zhang, Daili Feng, Lei Shi, Li Wang, Yingai Jin, Limei Tian, Ziyuan Li, Guoyong Wang, Lei Zhao, Yuying Yan, A review of phase change heat transfer in shape-stabilized phase change materials (ss-PCMs) based on porous supports for thermal energy storage, *Renewable and Sustainable Energy Reviews* 135 (2021) 110127.
13. Hafiz Muhammad Ali, Muhammad Mansoor Janjua, Uzair Sajjad, Wei-Mon Yan, A critical review on heat transfer augmentation of phase change materials embedded with porous materials/foams, *International Journal of Heat and Mass Transfer* 135 (2019) 649–673.
14. Qinlong Ren, Ya-Ling He, Kai-Zhi Su, Cho Lik Chan, Investigation of the effect of metal foam characteristics on the PCM melting performance in a latent heat thermal energy storage unit by pore-scale lattice Boltzmann modeling, *Numerical Heat Transfer, Part A: Applications* 72 (10) (2017) 745–764.
15. Xinyi Li, Cong Niu, Xiangxuan Li, Ting Ma, Lin Lu, Qiuwang Wang, Pore-scale investigation on effects of void cavity distribution on melting of composite phase change materials, *Applied Energy* 275 (2020) 115302.
16. Ya-Ling He, Wen-Quan Tao, Multiscale simulations of heat transfer and fluid flow problems, *Journal of Heat Transfer* 134 (3) (2012) 031018.
17. Li Chen, Yong-Liang Feng, Chen-Xi Song, Lei Chen, Ya-Ling He, Wen-Quan Tao, Multi-scale modeling of proton exchange membrane fuel cell by coupling finite volume method and lattice Boltzmann method, *International Journal of Heat and Mass Transfer* 63 (2013) 268–283.
18. Ruiyuan Zhang, Ting Min, Li Chen, Qinjun Kang, Ya-Ling He, Wen-Quan Tao, Pore-scale and multiscale study of effects of Pt degradation on reactive transport processes in proton exchange membrane fuel cells, *Applied Energy* 253 (2019) 113590.
19. Zi-Xiang Tong, Ming-Jia Li, Xi Chen, Ya-Ling He, Direct coupling between molecular dynamics and lattice Boltzmann method based on velocity distribution functions for steady-state isothermal flow, *International Journal of Heat and Mass Transfer* 115 (2017) 544–555.
20. Wen-Jing Zhou, Zhi-Qiang Yu, Zhong-Zhen Li, Ya-Ling He, Wen-Quan Tao, Molecular dynamics-continuum hybrid simulation for the impingement of droplet on a liquid film, *Numerical Heat Transfer, Part A: Applications* 68 (2015) 512–525.
21. Li Chen, Ya-Ling He, Qinjun Kang, Wen-Quan Tao, Coupled numerical approach combining finite volume and lattice Boltzmann methods for multi-scale multi-physicochemical processes, *Journal of Computational Physics* 255 (2013) 83–105.
22. Zi-Xiang Tong, Ya-Ling He, A unified coupling scheme between lattice Boltzmann method and finite volume method for unsteady fluid flow and heat transfer, *International Journal of Heat and Mass transfer* 80 (2015) 812–824.
23. Daili Feng, Yanhui Feng, Lin Qiu, Pei Li, Yuyang Zang, Hanying Zou, Zepei Yu, Xinxin Zhang, Review on nanoporous composite phase change materials: Fabrication, characterization, enhancement and molecular simulation, *Renewable and Sustainable Energy Reviews* 109 (2019) 578–605.
24. Yong Zhang, Edward J. Maginn, A comparison of methods for melting point calculation using molecular dynamics simulations, *The Journal of Chemical Physics* 136 (2012) 144116.
25. YangChun Zou, ShiKai Xiang, ChengDa Dai, Investigation on the efficiency and accuracy of methods for calculating melting temperature by molecular dynamics simulation, *Computational Materials Science* 171 (2020) 109156.
26. Sirlok Srinivasan, Mouhamad S. Diallo, Sandip K. Saha, Opeyemi A. Abass, Aayush Sharma, Ganesh Balasubramanian, Effect of temperature and graphite particles fillers on thermal conductivity and viscosity of phase change material *n*-eicosane, *International Journal of Heat and Mass Transfer* 114 (2017) 318–323.

27. Changpeng Lin, Zhonghao Rao, Thermal conductivity enhancement of paraffin by adding boron nitride nanostructures: A molecular dynamics study, *Applied Thermal Engineering* 110 (2017) 1411–1419.
28. Yinsheng Yu, Yubing Tao, Ya-Ling He, Molecular dynamics simulation of thermophysical properties of NaCl-SiO_2 based molten salt composite phase change materials, *Applied Thermal Engineering* 166 (2020) 114628.
29. Yinsheng Yu, Chenyang Zhao, Yubing Tao, Xi Chen, Ya-Ling He, Superior thermal energy storage performance of NaCl-SWCNT composite phase change materials: A molecular dynamics approach, *Applied Energy* 290 (2021) 116799.
30. Shiyi Chen, Gary D. Doolen, Lattice Boltzmann method for fluid flows, *Annual Review of Fluid Mechanics* 30 (1998) 329–364.
31. Li Chen, Qinjun Kang, Yutong Mu, Ya-Ling He, Wen-Quan Tao, A critical review of the pseudopotential multiphase lattice Boltzmann model: Methods and applications, *International Journal of Heat and Mass Transfer* 76 (2014) 210–236.
32. W. Miller, The lattice Boltzmann method: A new tool for numerical simulation of the interaction of growth kinetics and melt flow, *Journal of Crystal Growth* 230 (1–2) (2001) 263–269.
33. I. Rasin, W. Miller, S. Succi, Phase-field lattice kinetic scheme for the numerical simulation of dendritic growth, *Physical Review E* 72 (6) (2005) 066705.
34. Yaling He, Qing Liu, Qing Li, Wenquan Tao, Lattice Boltzmann methods for single-phase and solid-liquid phase change heat transfer in porous media: A review, *International Journal of Heat and Mass Transfer* 129 (2019) 160–197.
35. Rongzong Huang, Huiying Wu, An immersed boundary-thermal lattice Boltzmann method for solid-liquid phase change, *Journal of Computational Physics* 227 (2014) 305–319.
36. Wen-Shu Jiaung, Jeng-Rong Ho, Chun-Pao Kuo, Lattice Boltzmann method for the heat conduction problem with phase change, *Numerical Heat Transfer, Part B: Fundamentals* 39 (2001) 167–187.
37. Mohsen Eshraghi, Sergio D. Felicelli, An implicit lattice Boltzmann model for heat conduction with phase change, *International Journal of Heat and Mass Transfer* 55 (9–10) (2012) 2420–2428.
38. Rongzong Huang, Huiying Wu, Ping Cheng, A new lattice Boltzmann model for solid-liquid phase change, *International Journal of Heat and Mass Transfer* 59 (2013) 295–301.
39. Rongzong Huang, Huiying Wu, Phase interface effects in the total enthalpy-based lattice Boltzmann model for solid-liquid phase change, *Journal of Computational Physics* 294 (2015) 346–362.
40. Dong Li, Qinlong Ren, Zi-Xiang Tong, Ya-Ling He, Lattice Boltzmann models for axisymmetric solid-liquid phase change, *International Journal of Heat and Mass Transfer* 112 (2017) 795–804.
41. Yutao Huo, Zhonghao Rao, Investigation of solid-liquid phase change in the spherical capsule using axisymmetric lattice Boltzmann method, *International Journal of Heat and Mass transfer* 119 (2018) 1–9.
42. Dong Li, Zi-Xiang Tong, Qinlong Ren, Ya-Ling He, Wen-Quan Tao, Three-dimensional lattice Boltzmann models for solid-liquid phase change, *International Journal of Heat and Mass Transfer* 115 (2017) 1334–1347.
43. Qing Liu, Xiang-Bo Feng, Ya-Ling He, Cai-Wu Lu, Qing-Hua Gu, Three-dimensional multiple-relaxation-time lattice Boltzmann models for single-phase and solid-liquid phase-change heat transfer in porous media at the REV scale, *Applied Thermal Engineering* 152 (2019) 319–337.
44. Wen-Zhen Fang, Yu-Qing Tang, Chun Yang, Wen-Quan Tao, Pore scale investigations on melting of phase change materials considering the interfacial thermal resistance, *International Communications in Heat and Mass Transfer* 115 (2020) 104631.

45. Xinyi Li, Ting Ma, Jun Liu, Hao Zhang, Qiuwang Wang, Pore-scale investigation of gravity effects on phase change heat transfer characteristics using lattice Boltzmann method, *Applied Energy* 222 (2018) 92–103.
46. Moran Wang, Ning Pan, Modeling and prediction of the effective thermal conductivity of random open-cell porous foams, *International Journal of Heat and Mass Transfer* 51 (2008) 1325–1331.
47. Yan Su, Tiniao Ng, Yinping Zhang, Jane H. Davidson, Three dimensional thermal diffusion in anisotropic heterogeneous structures simulated by a non-dimensional lattice Boltzmann method with a controllable structure generation scheme based on discrete Gaussian quadrature space and velocity, *International Journal of Heat and Mass Transfer* 108 (2017) 386–401.
48. S. Abishek, A.J.C. King, R. Mead-Hunter, V. Golkarfard, W. Heikamp, B.J. Mullins, Generation and validation of virtual nonwoven, foam and knitted filter (separator/coalesce) geometries for CFD simulations, *Separation and Purification Technology* 188 (2017) 493–507.
49. Qinlong Ren, Zexiao Wang,Jianjun Zhu, Zhiguo Qu, Pore-scale heat transfer of heat sink filled with stacked 2D metal fiber-PCM composite, *International Journal of Thermal Sciences* 161 (2021) 106739.
50. Qinlong Ren, Cho Lik Chan, GPU accelerated numerical study of PCM melting process in an enclosure with internal fins using lattice Boltzmann method, *International Journal of Heat and Mass Transfer* 100 (2016) 522–535.
51. Qinlong Ren, Penghua Guo, Jianjun Zhu, Thermal management of electronic devices using pin-fin based cascade microencapsulated PCM/expand graphite composite, *International Journal of Heat and Mass Transfer* 149 (2020) 119199.
52. Wenquan Tao, *Numerical Heat Transfer*, 2nd ed., Xi'an Jiaotong University Press, Xi'an 2001.
53. Hossein Asgharian, Ehsan Baniasadi, A review on modeling and simulation of solar energy storage systems based on phase change materials, *Journal of Energy Storage* 21 (2019) 186–201.
54. D.L Sun, Zhiguo Qu, Yaling He, Wenquan Tao, An efficient segregated algorithm for incompressible fluid flow and heat transfer problems-IDEAL (inner doubly iterative efficient algorithm for linked equations) part I: Mathematical formulation and solution procedure, *Numerical Heat Transfer, Part B: Fundamentals* 53 (2008) 1–17.
55. Wenqiang Li, Zhiguo Qu, YaLing He, WenQuan Tao, Experimental and numerical studies on melting phase change heat transfer in open-cell metallic foams filled with paraffin, *Applied Thermal Engineering* 37 (2012) 1–9.
56. Kong Ling, Wen-Quan Tao, A sharp-interface model coupling VOSET and IBM for simulations on melting and solidification, *Computers and Fluids* 178 (2019) 113–131.
57. Jasim M. Mahdi, Emmanuel C. Nsofor, Melting enhancement in triplex-tube latent heat thermal energy storage system using nanoparticles-metal foam combination, *Applied Energy* 191 (2017) 22–34.
58. Yang Xu, Qinlong Ren, Zhang-Jing Zheng, Ya-Ling He, Evaluation and optimization of melting performance for a latent heat thermal energy storage unit partially filled with porous media, *Applied Energy* 193 (2017) 84–95.
59. Chenzhen Ji, Zhen Qin, Swapnil Dubey, Fook Hoong Choo, Fei Duan, Simulation on PCM melting enhancement with double-fin length arrangements in a rectangular enclosure induced by natural convection, *International Journal of Heat and Mass Transfer* 127 (2018) 255–265.
60. Fan Yuan, Ming-Jia Li, Yu Qiu, Zhao Ma, Meng-Jie Li, Specific heat capacity improvement of molten salt for solar energy applications using charged single-walled carbon nanotubes, *Applied Energy* 250 (2019) 1481–1490.

61. C.Y. Zhao, Y.B. Tao, Y.S. Yu, Molecular dynamics simulation of nanoparticle effect on melting enthalpy of paraffin phase change material, *International Journal of Heat and Mass Transfer* 150 (2020) 119382.
62. C.Y. Zhao, Y.B. Tao, Y.S. Yu, Molecular dynamics simulation of thermal and phonon transport characteristics of nanocomposite phase change material, *Journal of Molecular Liquids* 329 (2021) 115448.
63. Accelrys Inc., *Materials Studio*. San Diego, CA: Accelrys Software Inc., 2010.
64. William Humphrey, Andrew Dalke, Klaus Schulten, VMD: Visual molecular dynamics, *Journal of Molecular Graphics* 14 (1) (1996) 33–38.
65. Qinlong Ren, Enhancement of nanoparticle-phase change material melting performance using a sinusoidal heat pipe, *Energy Conversion and Management* 180 (2019) 784–795.
66. Qinlong Ren, Fanlong Meng, Penghua Guo, A comparative study of PCM melting process in a heat pipe-assisted LHTES unit enhanced with nanoparticles and metal foams by immersed boundary-lattice Boltzmann method at pore-scale, *International Journal of Heat and Mass Transfer* 121 (2018) 1214–1228.
67. Zhao-Li Guo, Chu-Guang Zheng, Bao-Chang Shi, Non-equilibrium extrapolation method for velocity and pressure boundary conditions in the lattice Boltzmann method, *Chinese Physics* 11 (2002) 366.
68. Zhaoli Guo, Chuguang Zheng, An extrapolation method for boundary conditions in lattice Boltzmann method, *Physics of Fluids* 14(6) (2002) 2007–2010.
69. Chih-Hao Liu, Kuen-Hau Lin, Hao-Chueh Mai, Chao-An Lin, Thermal boundary conditions for thermal lattice Boltzmann simulations, *Computers & Mathematics with Applications* 59 (7) (2010) 2178–2193.
70. Rui Du, Baochang Shi, Xingwang Chen, Multi-relaxation-time lattice Boltzmann model for incompressible flow, *Physics Letters A* 359 (2006) 564–572.
71. Di Tian, Zhiguo Qu, Jianfei Zhang, Qinlong Ren, Enhancement of solar pond stability performance using an external magnetic field, *Energy Conversion and Management* 243 (2021) 114427.
72. Moran Wang, Jinku Wang, Ning Pan, Shiyi Chen, Mesoscopic predictions of the effective thermal conductivity for microscale random porous media, *Physical Review E* 75 (2007) 036702.
73. Moran Wang, Jihuan He, Jianyong Yu, Ning Pan, Lattice Boltzmann modelling of the effective thermal conductivity for fibrous materials, *International Journal of Thermal Sciences* 46 (2007) 848–855.
74. Moran Wang, Qinjun Kang, Ning Pan, Thermal conductivity enhancement of carbon fiber composites, *Applied Thermal Engineering* 29 (2009) 418–421.
75. Qinlong Ren, Zexiao Wang, Tao Lai, JianFei Zhang, Zhiguo Qu, Conjugate heat transfer in anisotropic woven metal fiber-phase change material composite, *Applied Thermal Engineering* 189 (2021) 116618.
76. Qinlong Ren, Cho Lik Chan, Numerical study of double-diffusive convection in a vertical cavity with Soret and Dufour effects by lattice Boltzmann method on GPU, *International Journal of Heat and Mass Transfer* 93 (2016) 538–553.
77. Qinlong Ren, Chenxing Liang, Zexiao Wang, Zhiguo Qu, Continuous trapping of bacteria in non-Newtonian blood flow using negative dielectrophoresis with quadrupole electrodes, *Journal of Physics D: Applied Physics* 54 (2020) 015401.
78. Qinlong Ren, Chenxing Liang, Insulator-based dielectrophoretic antifouling of nanoporous membrane for high conductive water desalination, *Desalination* 482 (2020) 114410.
79. Qinlong Ren, Cho Lik Chan, Natural convection with an array of solid obstacles in an enclosure by lattice Boltzmann method on a CUDA computation platform, *International Journal of Heat and Mass Transfer* 93 (2016) 273–285.

80. Qinlong Ren, Yichao Wang, Xixiang Lin, Cho Lik Chan, AC electrokinetic induced non-Newtonian electrothermal blood flow in 3D microfluidic biosensor with ring electrodes for point-of-care diagnostics, *Journal of Applied Physics* 126 (2019) 084501.
81. Yao Zhao, Changying Zhao, Zhiguo Xu, Numerical study of solid-liquid phase change by phase field method, *Computers and Fluids* 164 (2018) 94–101.
82. Li Chen, Huibao Luan, Yongliang Feng, Chenxi Song, Ya-Ling He, Wen-Quan Tao, Coupling between finite volume method and lattice Boltzmann method and its application to fluid flow and mass transport in proton exchange membrane fuel cell, *International Journal of Heat and Mass Transfer* 55 (13–14) (2012) 3834–3848.
83. H.B. Luan, H. Xu, L. Chen, D.L. Sun, W.Q. Tao, Numerical illustrations of the coupling between the lattice Boltzmann method and finite-type macro-numerical methods, *Numerical Heat Transfer, Part B: Fundamentals* 57 (2010) 147–171.
84. Hui Xu, Huibao Luan, Yaling He, Wenquan Tao, A lifting relation from macroscopic variables to mesoscopic variables in lattice Boltzmann method: Derivation, numerical assessments and coupling computations validation, *Computers & Fluids* 54 (2012) 92–104.
85. Zhonghao Rao, Shuangfeng Wang, Feifei Peng, Molecular dynamics simulations of nano-encapsulated and nanoparticle-enhanced thermal energy storage phase change materials, *International Journal of Heat and Mass Transfer* 66 (2013) 575–584.
86. Hongtao Xu, Ning Wang, Chenyu Zhang, Zhiguo Qu, Meng Cao, Optimization on the melting performance of triplex-layer PCMs in a horizontal finned shell and tube thermal energy storage unit, *Applied Thermal Engineering* 176 (2020) 115409.
87. Ben Xu, Peiwen Li, Cho Lik Chan, Application of phase change materials for thermal energy storage in concentrated solar thermal power plants: A review to recent developments, *Applied Energy* 160 (2015) 286–307.



Taylor & Francis
Taylor & Francis Group
http://taylorandfrancis.com